

Synthesis and Characterization of MnZn Ferrite Nanoparticles with Improved Saturation Magnetization

Mingling Li^{1,2} · Haiyan Fang² · Honglin Li² · Yuyu Zhao² · Tianran Li² · Haibo Pang² · Jin Tang¹ · Xiansong Liu¹

Received: 3 February 2017 / Accepted: 6 February 2017 / Published online: 9 March 2017
© Springer Science+Business Media New York 2017

Abstract $\text{Mn}_{0.8}\text{Zn}_{0.2}\text{Fe}_2\text{O}_4$ nanoparticles with improved saturation magnetization were prepared by a modified hydrothermal method. This method involves a chemical coprecipitation of hydroxides under a vacuum condition using potassium hydroxide as a precipitating agent, followed by a separate hydrothermal process. To understand the advantages of the modified hydrothermal method proposed above, a sample having identical stoichiometry was prepared by conventional hydrothermal method, during which the preparation of precursor was conducted in an open system. The samples were characterized by XRD, X-ray photoelectron spectroscopy (XPS), Raman spectroscopy, and TEM. The magnetic property was tested by vibrating sample magnetometer (VSM). XPS results show that the Mn cations of the nanoparticles prepared by modified hydrothermal method have lower average valence. The MnZn ferrite nanoparticles prepared by modified hydrothermal method have smaller diameter (16.1 nm, calculated by XRD) and higher room temperature saturation magnetization, 80 emu/g, which is even better than the reported value. The saturation magnetization of the particles prepared by modified hydrothermal method is 1.6 times of the particles prepared by conventional hydrothermal method.

Keywords Magnetic nanoparticles · MnZn ferrite · Modified hydrothermal method · Saturation magnetization

1 Introduction

Nowadays, nanostructured magnetic materials, especially the ferrite nanoparticles, have been a topic of active investigations in the magnetism research, mainly due to the unique magnetic properties that do not present for the microscopic scale or bulk materials. MnZn ferrite, one of the most important soft ferrites, is widely used in many fields presently as deflection rings, computer memory chips, microwave devices, transducers, transformers, and so on, for presenting high magnetic permeability, high saturation magnetization, low coercivity, low power losses, high chemical stability, etc. [1]. Additionally, nanosized MnZn ferrite particles can be manipulated by external magnetic fields, so they present a great potential market and broad application prospect in the fields as magnetic separation, catalysis, hyperthermia, ferrofluids, bioseparation, and targeted drug delivery [2].

These abovementioned applications require not only smaller size nanoparticles, but also high magnetization. The development of MnZn ferrite nanoparticles has been intensively pursued in recent years for their technological and fundamental scientific importance, and many efforts have been made to gain nanosized MnZn ferrite with superior microstructure, morphology, and magnetic properties. As is well known, the morphology and properties of MnZn ferrite nanoparticles are significantly influenced by synthesis method. Therefore, various techniques on the synthesis of the nanosized ferrites have been proposed, such as coprecipitation, sol-gel, microemulsion method, polymeric precursor method, microwave-assisted combustion, thermal deposition of precursors, and hydrothermal reactions

✉ Xiansong Liu
xiansongliu@ahu.edu.cn

¹ School of Physics and Materials Science, Anhui University, Hefei, 230601, Anhui, People's Republic of China

² Institute of New Functional Materials and Fine Chemicals Research, Chaohu University, Hefei, 238000, People's Republic of China

[3–6]. Among these, the hydrothermal method has become one of the favorable and promising methods to synthesize improved performance nanosized ferrites. The most significant distinction of hydrothermal method is that the nanopowders can be obtained at relatively low temperature with high crystallinity and without additional heat treatment process.

It has been more than 100 years since the hydrothermal method was used to prepare ferrite materials. In such a long time, researches on the improvement of hydrothermal method have never been stopped. Till now, despite a lot of relevant reports, the amelioration of hydrothermal method is still an important research topic. The improvements mainly focus on boosting the kinetics of the reaction or optimizing the experimental conditions to obtain suitable ferrite nanoparticles [7, 8].

There are some common characteristics in the preparation of MnZn ferrite nanoparticles using hydrothermal methods, such as the use of metal nitrate or chlorides as precursors, autoclave synthesis at low reaction temperatures 140–190 °C and pH 9–12. However, the properties of the obtained ferrite nanoparticles are very different. According to the professional documents, the reported saturation magnetization value of nanosized MnZn ferrites is between 10 and 60 emu/g, far less than that of the bulk MnZn ferrite materials [9–11]. This situation greatly limits the application of MnZn ferrite nanoparticles in the fields as chemistry, chemical industry, and biomedicine. Therefore, there is a long way to go for the high performance of nanosized MnZn ferrites. In this article, a modified hydrothermal method is proposed for the first time to prepare high-performance MnZn ferrite nanoparticles, during which the fabrication of precursor comprised of hydroxides is conducted under a vacuum condition, then followed by a separate hydrothermal crystallization process as same as that of traditional hydrothermal method. We investigated the structure and properties of the products and analyzed the reasons for the improvement of performance by comparing with the traditional hydrothermal method.

2 Experimental Procedure

2.1 Synthesis

Nanosized $\text{Mn}_{0.8}\text{Zn}_{0.2}\text{Fe}_2\text{O}_4$ ferrite particles were synthesized by a modified hydrothermal method which consisted of two steps: the preparation of precursors under vacuum conditions and followed by a separate hydrothermal process. Commercially AR-grade ferric nitrate ($\text{Fe}(\text{NO}_3)_3 \cdot 9\text{H}_2\text{O}$, 98.5 %), zinc sulfate heptahydrate ($\text{ZnSO}_4 \cdot 7\text{H}_2\text{O}$, 99.5 %), manganese(II) sulfate monohydrate ($\text{MnSO}_4 \cdot \text{H}_2\text{O}$, 99 %), and potassium hydroxide (KOH, 82 %) were

used as starting materials in the present work without any further purification. Initially, 1.6406 g $\text{Fe}(\text{NO}_3)_3 \cdot 9\text{H}_2\text{O}$ (4 mmol), 0.1156 g $\text{ZnSO}_4 \cdot 7\text{H}_2\text{O}$ (0.4 mmol), and 0.2732 g $\text{MnSO}_4 \cdot \text{H}_2\text{O}$ (1.6 mmol) were dissolved in 25 ml deionized water, and a mixed salt solution was obtained. In addition, 1.344 g KOH (24 mmol) was dissolved in 10 ml deionized water and used as precipitating agent. Under vacuum conditions, the KOH solution was slowly added into the salt solution with stirring, resulting in a precursor comprised of hydroxide precipitation. Then the precursor was poured into a Teflon-lined stainless steel autoclave quickly, and the volume of the resultant solution was around 30 % of the autoclave total volume. After heating at 180 °C for 3 h, the autoclave was cooled down to room temperature naturally. The as-synthesized powders were taken out and washed several times with deionized water and ethanol, then the wet slurry was kept in a vacuum oven for 5 h at 80 °C. The resulting sample was named MZF-m. A reference sample having the same chemical composition was synthesized via a conventional hydrothermal method, the only difference of which, compared with the modified hydrothermal method previously mentioned, is that the preparation of the precursor was carried out in an open system. The sample prepared by conventional hydrothermal method was labeled as MZF-c, and its microstructure and magnetic property were tested and compared to that of the samples MZF-m to illustrate the effect of synthesis condition on the structure and magnetic property.

2.2 Sample Characterization

Phase formation of the samples was investigated by X-ray diffraction (XRD) method by using $\text{Cu K}\alpha$ radiation ($\lambda = 0.154 \text{ nm}$) and scanning range of $2\theta = 10^\circ$ to 70° (Dmax 2500 XRD diffractometer) at a continuous scanning rate of $10^\circ/\text{min}$. The phase identification was made by comparing powder diffractograms with standard patterns from the Inorganic Crystal Structure Database (ICSD). In addition, the peaks were employed to calculate the particle size (D) of the samples using the Debye–Scherrer's equation: $D = 0.89 \cdot \lambda / \beta \cos \theta$, where λ is the X-ray wavelength, β is full width at half the maxima (FWHM), and θ is Bragg's angle. An inVia Raman microscope (HR Evolution) was used to record the chemical structure of sample MZF-m. An argon ion laser at 785 nm was used as excitation source. The sample was placed in 1.0-mm (inside diameter) quartz capillaries. The experimental conditions were as follows: 1 mW power, a $\times 100$ objective microscope, 1 cm^{-1} spectral resolution, and $30 \text{ s} \times 3$ collection time. The XPS measurements were carried out using a Thermo-Fisher ESCALAB 250Xi using $\text{Al K}\alpha$ X-ray source and a 150-mm hemispherical analyzer with 20 eV pass energy and operating at 1486.8 eV during the measurement. Charge shift was

corrected by adjusting the binding energy C1s to 284.8 eV. The peak-fit processing was used with XPSPEAK program at a Lorentzian to Gaussian ratio of 80 % after the subtraction of Shirley-type background. Particle morphology was checked using a high resolution transmission electron microscopy (HRTEM, Model JEM-2010). Hysteresis loops were measured by a Lakeshore Model 7404 vibrating sample magnetometer (VSM) at room temperature with an applied field $-10 \text{ kOe} \leq H \leq 10 \text{ kOe}$, and the saturation magnetization (M_s) of the samples was calculated in terms of the hysteresis loops.

3 Results and Discussion

3.1 XRD

XRD patterns of the as-prepared ferrite samples are shown in Fig. 1. The diffraction peaks match well with those of the spinel MnZn ferrite, $\text{Mn}_{0.8}\text{Zn}_{0.2}\text{Fe}_2\text{O}_4$ (ICSD no. 74-2402), and no other peaks are found in the XRD patterns. The observed diffraction peaks are indexed. The results indicate that the samples prepared at different conditions are pure MnZn ferrite with cubic spinel structure. In addition, from the appearance of the XRD diffractograms, broad and low intensity, it is obvious that the samples have very small particle size. The XRD patterns of the two samples look macroscopically the same but have subtle difference in the 2θ values, which denote different unit cell sizes. The lattice constants and particle sizes were calculated from XRD patterns as given in Fig. 2. It is noticed that the value of the lattice constant of MZF-m is larger than that of MZF-c, while the crystallites' size of MZF-m is smaller than

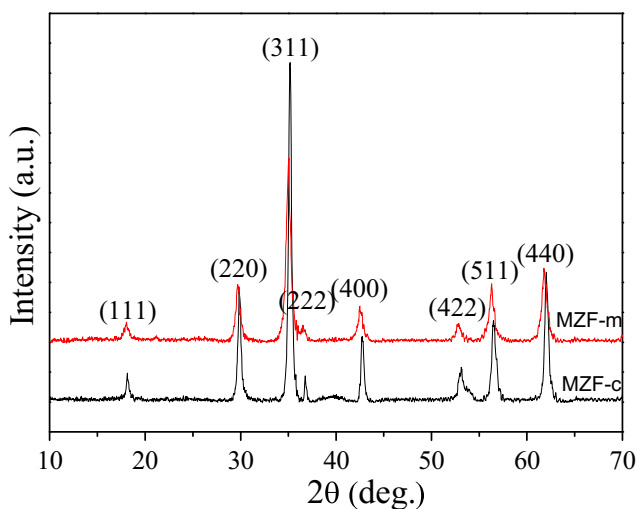


Fig. 1 X-ray diffraction patterns of the $\text{Mn}_{0.8}\text{Zn}_{0.2}\text{Fe}_2\text{O}_4$ nanoparticles synthesized by modified hydrothermal method (MZF-m) and conventional hydrothermal method (MZF-c)

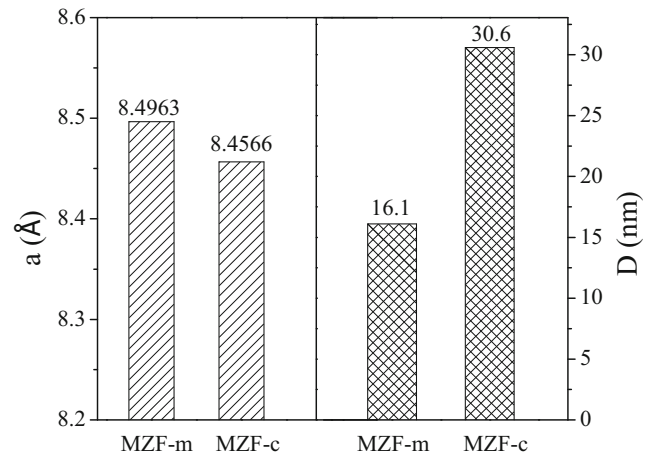


Fig. 2 Comparison graph of lattice parameter (a) and particle size (D) of different samples

that of MZF-c. The lattice constant of nanosized MnZn ferrite prepared by modified hydrothermal method (8.4963 Å) is very close to the theoretical value of $\text{Mn}_{0.8}\text{Zn}_{0.2}\text{Fe}_2\text{O}_4$ (8.5136 Å). The decrease in the lattice constant of nanosized MnZn ferrite prepared by conventional hydrothermal method could be attributed to the presence of Mn^{3+} (0.645 Å) and Mn^{4+} (0.54 Å) ions in octahedral sites with a smaller ionic size compared with Mn^{2+} (0.82 Å) [12]. It is well known that manganese hydroxide ($\text{Mn}(\text{OH})_2$) is quickly oxidized in the air, even if trace oxygen dissolved in water can oxidize manganese hydroxide. Thus, according to the XRS results, the oxidation of the divalent manganese ions can be avoided to a certain extent during the preparation of precursors by the modified hydrothermal method which provides a vacuum environment during the preparation of precursor.

3.2 Raman Spectrum

Spinel ferrite has the general chemical formula MeFe_2O_4 , where Me is divalence metal ions or a mixture of ions having average valence of two. The oxygen ions form a nearly close-packed face centered cubic structure generating tetrahedral (A sites) and octahedral (B sites) local symmetry. The distribution of metal ions over A or B sites is governed by relative site preference and energies of cations present, which control the intrinsic properties of ferrites. On the basis of cations distribution, ferrites can be classified into three categories: normal ferrites, inverse ferrites, and mixed ferrites. MnZn ferrite is a mixed spinel ferrite with the $Fd3m$ space group, in which the divalent ions occupy both A and B sites. It is predicted from the group theory analysis that the spinel MnZn ferrite has five first-order modes such as $1A_{1g}$, $1E_g$, and $3T_{2g}$ possessing Raman activity [13]. Hence,

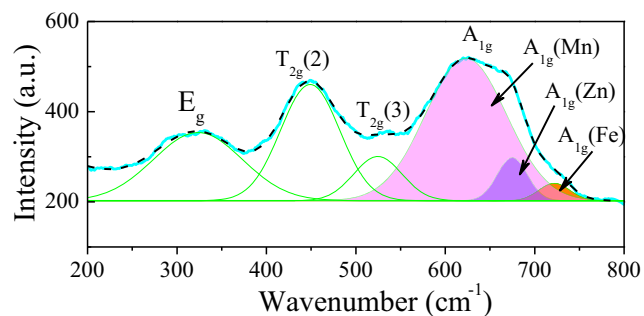


Fig. 3 Raman spectra of $\text{Mn}_{0.8}\text{Zn}_{0.2}\text{Fe}_2\text{O}_4$ ferrite nanoparticles synthesized by modified hydrothermal method (sample MZF-m)

Raman spectroscopy can be used to reveal the molecular structure of MnZn ferrite nanoparticles.

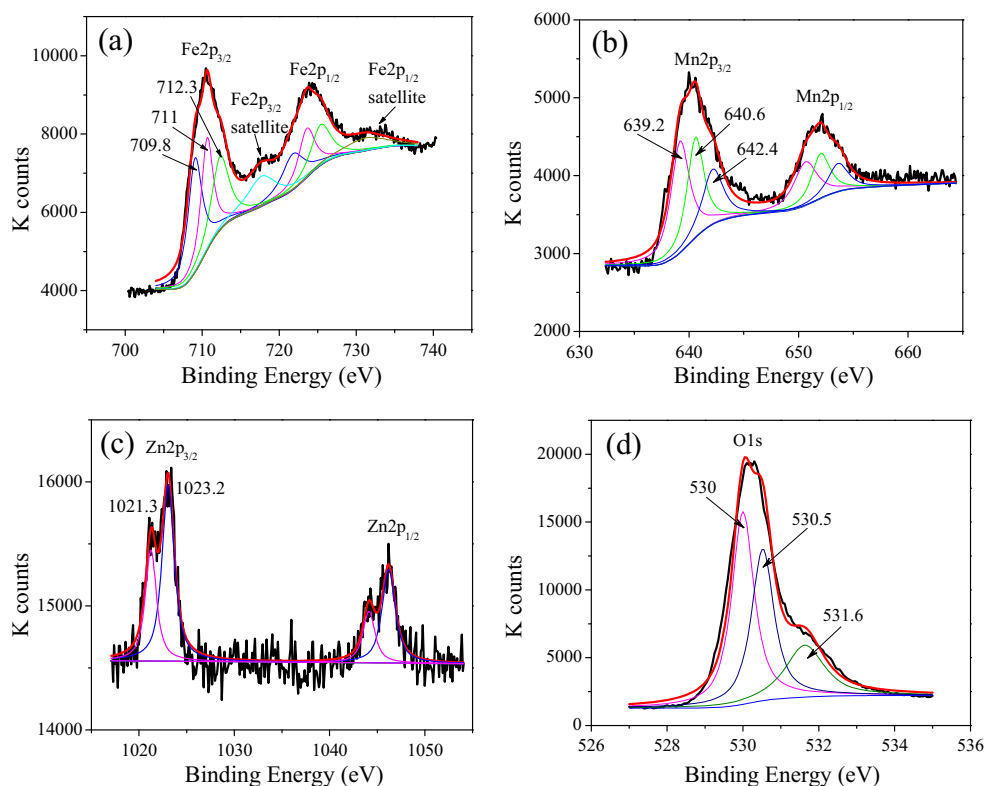
Raman spectrum of the sample MZF-m was recorded at room temperature in the energy range of 200 to 800 cm^{-1} and shown in Fig. 3. To analyze the molecular structure more accurately, the obtained Raman spectrum has been deconvoluted into individual Lorentzian peaks. It is seen that there are four obvious first-order Raman modes peaked at ~ 320 , ~ 450 , ~ 520 , and ~ 720 cm^{-1} corresponding to E_g , $T_{2g}(2)$, $T_{2g}(3)$, and A_{1g} , respectively. The peak $T_{2g}(1)$ (~ 160 cm^{-1}) falls beyond the range of study, and therefore, could not be recorded. The appearance of the remaining four peaks is in agreement with the previous reported data of MnZn ferrite nanoparticles [14]. The recorded Raman

spectrum of sample MZF-m confirms the formation of cubic spinel MnZn ferrite and rules out the existence of the impurity phase $\alpha\text{-Fe}_2\text{O}_3$, which usually gives strong bands at ~ 240 and ~ 300 cm^{-1} [15]. In addition, the mode above 600 cm^{-1} , corresponding to the tetrahedral sub-lattices stretches, splits into three different energy levels appearing at 620, 660, and 720 cm^{-1} (Fig. 3). The three deconvoluted peaks correspond to tetrahedrally coordinated Mn-O, Zn-O, and Fe-O stretches, respectively, and this phenomenon suggests that Mn, Zn, and Fe occupy A sites. However, the relative area of the three peaks in this paper is different from that reported in the literature [14], which could be interpreted that the modified hydrothermal method has some influence on the cation distribution.

3.3 XPS

X-ray photoelectron spectroscopy (XPS), a versatile surface analysis technique, is widely used to analyze compositional and chemical states. Detailed surface studies of the nanoparticles were carried out by XPS to check the chemical states of each element of the MnZn ferrite samples. The Fe2p, Mn2p, Zn2p, and O1s photoelectron spectra of the sample MZF-m are shown in Fig. 4a–d. It can be seen from Fig. 4a that the Fe2p peaks are composed of two main asymmetric peaks: Fe2p_{3/2} and Fe2p_{1/2}, with a binding energy at 710.5 and 723.8 eV, respectively, and the doublet spacing

Fig. 4 XPS analysis of MnZn ferrite nanoparticles prepared by a modified hydrothermal method: **a** fitted Fe2p_{1/2} and Fe2p_{3/2} photoelectron peaks; **b** fitted Mn2p_{1/2} and Mn2p_{3/2} photoelectron peaks; **c** fitted Zn2p_{1/2} and Zn2p_{3/2} photoelectron peaks, and; **d** fitted O1s photoelectron peaks



is 13.3 eV. In addition, the two small peaks located at about 718.8 and 731 eV are the satellite peaks of Fe2p_{3/2} and Fe2p_{1/2}, respectively. This phenomenon reveals that Fe³⁺ is the only oxidation state present on the nanoparticle surface/near-surface [16]. For Fe2p_{3/2} peak, three contributions at about 709.8, 711, and 712.3 eV reflect three different circumstances of Fe³⁺ ions. Peaks at 709.8 and 711 eV can be attributed to the Fe³⁺ cations with different occupancies (tetrahedral or octahedral) in the spinel ferrite, while the higher binding energy at about 712.3 eV is assigned to Fe³⁺ bonded with hydroxyl groups [16, 17]. Two asymmetric peaks located around 641 and 652 eV (seen in Fig. 4b) correspond to Mn2p_{3/2} and Mn2p_{1/2}, respectively. The Mn2p_{3/2} can be deconvoluted into three contributions and the binding energies are 639.2, 640.6, and 642.4 eV, respectively. Peng Liu et al. studied the chemical state of Mn by XPS, and they deconvoluted the Mn2p_{3/2} peak into three contributions centered at 641.4, 642.5, and 643.8 eV, corresponding to Mn³⁺, Mn⁴⁺, and Mn cations bonded with hydroxyl groups, respectively [18]. It can be noticed that there is a reduction in the binding energy of each chemical state of Mn ions in our sample MZF-m compared with that of Peng Liu and co-workers. The decrease of binding energy confirms the lower average valence of Mn cations in the sample MZF-m. Thus, the Mn2p_{3/2} peaks at 639.2 eV can be attributed to the Mn^{x+} ($2 < x < 3$) cations and 640.6 eV can be attributed to the Mn^{y+} ($3 < y < 4$) cations. The Mn2p photoelectron spectrum shows that there is no Mn²⁺ on the nanoparticle surface for the absence of a satellite feature at about 647 eV, which is characterized only by MnO.

Figure 4c is the photoelectron spectrum and fitting results of Zn2p in nanoparticles of sample MZF-m. It is obvious that the Zn2p_{3/2} splits into two peaks centered at 1021.3 and 1023.2 eV, the energy value is consistent with the results reported by Bera et al. [19]. The peaks at 1021.3 eV are ascribed to the zinc cations occupying tetrahedral sites, and 1023.2 eV is ascribed to the zinc cations occupying octahedral sites, which has been reported by Druska et al. [20], who observed the Zn cations occupying octahedral sites as a result of mechanical treatment on the normal zinc ferrite. However, the Zn2p_{3/2} peak in this paper, different from the shape reported in the literature [19], split into two distinct peaks. The formation of the special Zn2p_{3/2} peak in sample MZF-m may be due to the improvement of ordering degree of Zn²⁺.

The high resolution spectrum for O1s, as presented in Fig. 4d, shows three oxygen contributions, peaking at 530, 530.5, and 531.6 eV, respectively. The component O1s sitting at 530 and 530.5 eV is commonly associated with metal-oxygen bonds (the lattice oxygen), while the fitting peak of O1s at 531.6 eV is contributed to the surface absorbed oxygen [21].

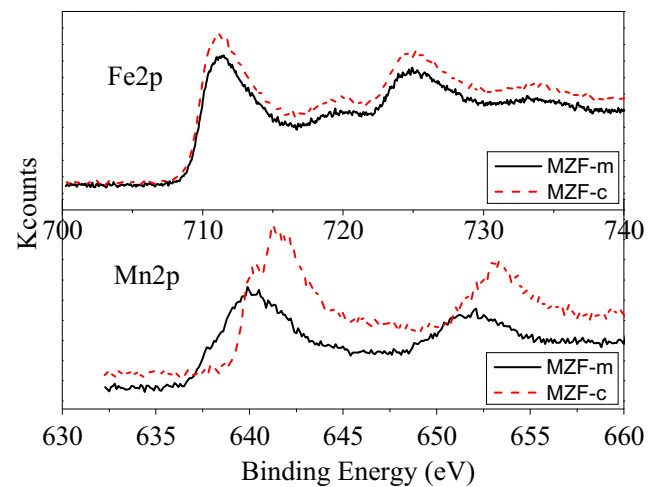


Fig. 5 Comparison graph of Fe2p and Mn2p photoelectron peaks of MnZn ferrite nanoparticles prepared by different method

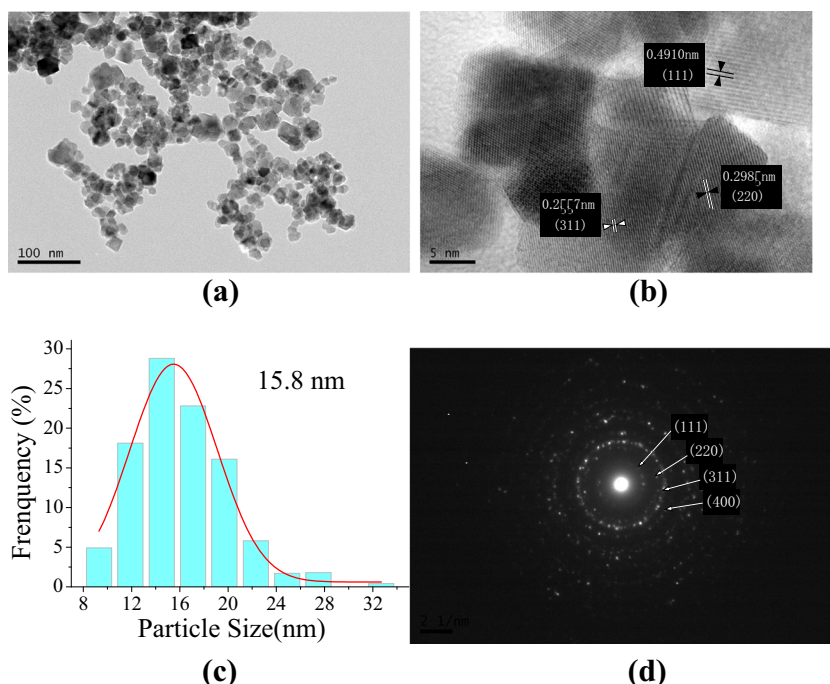
The XPS data demonstrates that the surface of the sample MZF-m prepared by a modified hydrothermal method has a composition containing Mn^{x+} ($2 < x < 3$), Mn^{y+} ($3 < y < 4$), Zn²⁺, Fe³⁺, and O²⁻; furthermore, there is a part of Zn²⁺ occupying the octahedral sites on the particles surface, which is different from the grain interior.

To intuitively observe the difference of the ions' chemical state in samples MZF-m and MZF-c, the photoelectron peaks of Fe2p and Mn2p in two samples were listed in Fig. 5. It can be seen that there is almost no difference in the Fe2p photoelectron spectra between samples MZF-m and MZF-c, while the doublet of Mn2p in sample MZF-m exhibited a shift by 1.5 eV towards lower binding energy compared to the Mn2p doublet of sample MZF-c, which could be interpreted that the average valence of Mn ions in sample MZF-m is lower than in sample MZF-c, and that the chemical state of Mn cations on the particles surface of sample MZF-m can be expressed as Mn^{x+} ($2 < x < 3$) and Mn^{y+} ($3 < y < 4$).

3.4 TEM

TEM micrographs of the obtained MnZn ferrite nanoparticles prepared by the modified hydrothermal method (sample MZF-m) at low and high magnifications are shown in Fig. 6a–d. The particles are nearly spherical in shape with a uniform distribution. The particles size is shown in the histogram (Fig. 6c), which is obtained from the TEM micrograph using a soft nanomeasurer. The average diameter is estimated from the lognormal distribution fitted by the preceding histogram, and the value is 15.8 nm, agreeing closely with the particle size calculated from XRD (16.1 nm). The HRTEM image (Fig. 6b) reveals that the particles in sample MZF-m are polycrystalline. Figure 6d is the selected

Fig. 6 Microstructural analysis of sample MAF-m: **a** TEM micrograph, **b** HRTEM image, **c** histogram, and **d** selected area electron diffraction pattern (SAED)



electron diffraction pattern, obtained from the area shown in Fig. 6a. The diffuse intensity and its distribution verify the nanocrystallinity of the particles and the rings on the diffraction pattern are typical crystal structure of MnZn ferrite.

3.5 VSM

The room-temperature hysteresis loops of the MnZn ferrite nanoparticles synthesized by different methods (MZF-m and MZF-c) were measured in the form of powders and are shown in Fig. 7, and the inset shows the coercivity of samples. The saturation magnetization of sample MZF-m (16.1 nm) is 80 emu/g while that of sample MZF-c (30.6 nm) is only 48 emu/g, which indicates that the value of saturation magnetization raises about 70 % when processing is changed from conventional hydrothermal method to the modified one. In addition, the remanence and coercivity of sample MZF-m are far less than that of sample MZF-c (the inset of Fig. 7). The sample MZF-m exhibited high Ms and low Hc in this study. The results obtained above confirm that the modified hydrothermal method first proposed present more advantages over the conventional hydrothermal method. Furthermore, the Ms value of sample MZF-m is obviously higher than that of the MnZn ferrite nanopowders with identical composition synthesized using other methods, and the Hc is much lower [10, 11, 22, 23].

Many researches indicate that the particle size has a critical influence on the saturation magnetization of magnetic nanoparticles. In general, the saturation magnetization increases with the increase of particle size for the rotation

of the domain walls in large particles is easier. By contrast, however, the particle size of sample MZF-m (16.1 nm) is smaller than that of MZF-c (30.6 nm) and the saturation magnetization is higher. Thus, it is not correct to evaluate the magnetization of the nanoparticles only according to the particles size. In general, the saturation magnetization of ferrites is fairly depend on the crystallinity, impurity, cation distribution, and particle size, because these factors will directly affect the exchange interaction between the metal ions in A and B sites, and at the same time,

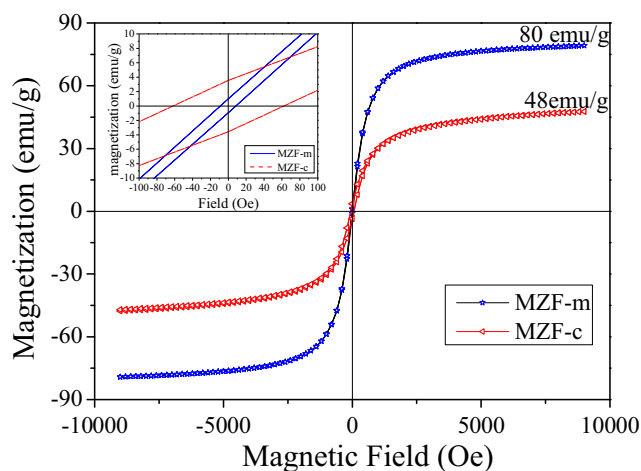


Fig. 7 Hysteresis loops (300 K) of samples prepared under different conditions: MZF-m by modified hydrothermal method and MZF-c by conventional hydrothermal method. *Inset* magnetization at low magnetic fields

these factors are greatly influenced by the synthesis processes. In this study, the magnetic properties of sample MZF-m were greatly improved, and the principal cause could be due to the decrease of the degree of oxidation of magnetic Mn^{2+} cations by providing a vacuum atmosphere during the preparation of precursor, because the magnetic moment of Mn^{2+} is larger than that of M^{3+} and M^{4+} , as well as the ion distribution was modified in the new process.

4 Conclusion

$\text{Mn}_{0.8}\text{Zn}_{0.2}\text{Fe}_2\text{O}_4$ ferrite nanoparticles with narrow size distribution and high saturation magnetization were prepared by a modified hydrothermal method, which involves chemical co-precipitation of hydroxides under vacuum condition using potassium hydroxide as precipitating agent, followed by a hydrothermal processing. To understand the superiority of the modified hydrothermal method, a sample having identical stoichiometry was prepared by conventional hydrothermal method. The samples were characterized by XRD, XPS, HRTEM, Raman spectra, and VSM. The results reveal that the nanoparticles prepared by modified hydrothermal method have smaller diameter (16.1 nm, calculated by XRD) and higher room temperature saturation magnetization (80 emu/g). These findings are believed to provide further comprehension on the relations among the structure, magnetic properties, and synthesis conditions, as well as to raise an effective and simple method for preparing MnZn ferrite nanoparticles with improved magnetic properties. The application field will be further broadened by the successful preparation of MnZn ferrite nanoparticles with high saturation magnetization.

Acknowledgments This work was supported by the National Natural Science Foundation of China (grant no. 51472004), the program of Co-operative Innovation Research Center for Weak Signal-Detecting Materials and Devices Integration of Anhui University (grant no. 01001795-2014-02), and the National Training Program of Innovation and Entrepreneurship for Undergraduates (grant no. 2016103801623).

References

- Mohseni, H., Shokrollahi, H., Sharifi, I., Gheisari, K.: *J. Magn. Mater.* **324**, 3741–3747 (2012)
- Yoo, D., Lee, J.H., Shin, T.H.: *J. Cheon. Acc. Chem. Res.* **44**, 863–874 (2011)
- Hua, F., Yin, C.C., Zhang, H.Q., Suo, Q.Q., Wang, X., Peng, H.F.: *J. Mater. Sci. Chem. Eng.* **3**, 23–29 (2015)
- Thakur, A., Singh, M.: *Ceram. Int.* **29**, 505–511 (2003)
- Hu, P., Yang, H.B., Pan, D.A., Wang, H., Tian, J.J., Zhang, S.G.: *J. Magn. Magn. Mater.* **322**, 173–177 (2010)
- Pemartin, K., Solans, C., Alvarez, J.Q., Sanchez, M.D.: *Colloids Surf. A Physicochem. Eng. Asp.* **451**, 161–171 (2014)
- Lai, Z.Y., Lu, Z.Y., Liu, M., Sun, R.: *Electronic Components and Materials* **26**, 52–54 (2007)
- Lai, Z.Y., Xu, G.L., Liu, M.: *Journal of Southwest University of Science and Technology* **22**, 20–24 (2007)
- Freire, R.M., Freitas, P.G.C., Ribeiro, T.S., Vasconcelos, I.F., Denardin, J.C., Mele, G., Carbone, L., Mazzetto, S.E., Fachine, P.B.A.: *Microfluid. Nanofluid.* **17**, 233–244 (2014)
- Meng, Y.Y., Liu, Z.W., Dai, H.C., Yu, H.Y., Zeng, D.C., Shukla, S., Ramanujan, R.V.: *Powder Technol.* **229**, 270–275 (2012)
- Angermann, A., Topfer, J., Silva, K.L., Becker, K.D.: *J. Alloys. Compd.* **508**, 433–439 (2010)
- Syue, M.R., Wei, F.J., Chou, C.S., Fu, C.M.: *J. Appl. Phys.* **109**, 318–324 (2011)
- Kreisel, J., Lucazeau, G., Vincent, H.: *J. Solid State Chem.* **137**, 127–137 (1998)
- Thota, S., Subhash, C.K., Shiv, K.S., Reddy, V.R.: *J. Phys. Chem. Solids.* **91**, 136–144 (2016)
- de Faria, D.L.A., Venancio Silva, S., Oliveira, M.T.: *J. Raman Spectrosc.* **28**, 873–878 (1997)
- Yang, S.J., Guo, Y.F., Yan, N.Q., Wu, D.Q., He, H.P., Qu, Z., Jia, J.P.: *Ind. Eng. Chem. Res.* **50**, 9650–9656 (2011)
- Corkhill, C.L., Wincott, P.L., Lloyd, J.R., Vaughan, D.J.: *Geochim. Cosmochim. Acta.* **72**, 5616–5633 (2008)
- Liu, P., He, H.P., Wei, G.L., Liang, X.L., Qi, F.H., Tan, F.D., Tan, W., Zhu, J.X., Zhu, R.L.: *Appl. Catal. B Environ.* **182**, 476–484 (2016)
- Bera, S., Prince, A.A.M., Velmurugan, S., Raghavan, P.S., Gopalan, R., Panneerselvam, G., Narasimhan, S.V.: *J. Mater. Sci.* **36**, 5379–5384 (2001)
- Druska, P., Steinike, U., Sepelak, V.: *J. Solid State Chem.* **146**, 13–21 (1999)
- Li, S.D., Wang, H.S., Li, W.M., Wu, X.F., Tang, W.X., Chen, Y.F.: *Appl. Catal. B Environ.* **166**, 260–269 (2015)
- Murugesan, C., Chandrasekaran, G.: *J Supercond Nov Magn.* doi:10.1007/s10948-016-3604-1
- Cao, X., Liu, G., Wang, Y., Li, J.H., Hong, R.: *J. Alloys. Compd.* **497**, 9–12 (2010)